Role of Intersecting Equatorial and Coastal Waveguides Near Sri Lanka on Intraseasonal Sea Level Variability Along the West Coast of India

Iyyappan Suresh, Jérôme Vialard, Takeshi Izumo, Matthieu Lengaigne

JGR Oceans

RESEARCH ARTICLE
10.1029/2023JC020198

Role of Intersecting Equatorial and Coastal Waveguides Near Sri Lanka on Intraseasonal Sea Level Variability Along the West Coast of India

Iyyappan Suresh[1,2], **Jérôme Vialard**[3], **Takeshi Izumo**[4], **and Matthieu Lengaigne**[5]

[1]CSIR-National Institute of Oceanography (CSIR-NIO), Dona Paula, Goa, India, [2]Digital University Kerala (DUK), Trivandrum, Kerala, India, [3]LOCEAN-IPSL, Sorbonne Université-CNRS-IRD-MNHN, Paris, France, [4]Institut de Recherche pour le Développement (IRD), UMR241 SECOPOL (ex-EIO) laboratory, Université de la Polynésie Française (UPF), Tahiti, French Polynesia, [5]MARBEC, University of Montpellier, CNRS, IFREMER, IRD, Sète, France

Abstract The sea level variations along the west coast of India (WCI) significantly affect the ecosystems and fisheries, because of their tight coupling with the oxycline depths in this region, which hosts the world's largest natural hypoxic system. Here, we investigate the main causes of the WCI sea level variability. Using idealized experiments with a linear, continuously stratified ocean model, we first demonstrate that there is a direct pathway between the equatorial waveguide and the WCI, in addition to the well-documented pathway that aligns with the coastal waveguide in the Bay of Bengal. This direct connection results from the intersection of equatorial and coastal waveguides near Sri Lanka. The forced and reflected equatorial Rossby waves induce sea level variations at the Sri Lankan coast around 6°N, which propagate directly to the WCI as coastal Kelvin waves, without transiting through the Bay of Bengal coastal waveguide. Using model experiments with realistic coastline and forcing, we then illustrate that this direct pathway is the primary contributor (0.4 regression coefficient) to the WCI intraseasonal (20–150 days) sea level variability, followed by the Bay of Bengal coastal waveguide pathway (0.3) and the wind forcing in a small region near Sri Lanka (0.25). The remote forcing originating from the rest of the Bay of Bengal and the WCI local wind forcing have weaker influence. We conclude by discussing why this direct connection exhibits strong impact on sea level variability at the intraseasonal timescale, while its influence is considerably weaker at the longer seasonal and interannual timescales.

Plain Language Summary Sea level reflects variations in subsurface oceanic heat content and structure. Along the west coast of India (WCI), it acts as a warning sign for sudden strong decrease in seawater oxygen content that has deleterious impacts on ecosystems and fisheries. It is thus important to understand the causes of sea level variations in this region. Previous studies emphasized that equatorial wind variations force sea level anomalies that travel eastward, reach the Indonesian coast, and then propagate counter clockwise around the Bay of Bengal rim, around Sri Lanka and to the WCI. Here, we demonstrate that there is also a much shorter, direct pathway from the equatorial band to Sri Lankan coast and then to the WCI, bypassing the pathway through the Bay of Bengal. This newly discovered direct connection is in fact the primary contributor to WCI intraseasonal (20–150 days) sea level variations. The "classical" Bay of Bengal pathway is the second contributor. We also identify a forcing "hotspot" over a small region east of Sri Lanka as the third contributor. Finally, we demonstrate that the "direct" connection that we have highlighted here does not operate efficiently for sea level variations that span over a season or longer.

Key Points:

- This study highlights a new pathway for propagation of signals from equatorial band directly to west coast of India, bypassing Bay of Bengal
- This direct connection results from intersection of equatorial and coastal waveguides near Sri Lanka
- This pathway contributes to the west coast of India sea level primarily at intraseasonal timescale, but weakly at longer timescales

Supporting Information:

Supporting Information may be found in the online version of this article.

Correspondence to:

I. Suresh and J. Vialard,
i.suresh@duk.ac.in;
isuresh.nio@gmail.com;
jerome.vialard@ird.fr

Citation:

Suresh, I., Vialard, J., Izumo, T., & Lengaigne, M. (2024). Role of intersecting equatorial and coastal waveguides near Sri Lanka on intraseasonal sea level variability along the west coast of India. *Journal of Geophysical Research: Oceans*, *129*, e2023JC020198. https://doi.org/10.1029/2023JC020198

Received 2 JULY 2023
Accepted 13 FEB 2024

Author Contributions:

Conceptualization: Iyyappan Suresh, Jérôme Vialard
Formal analysis: Iyyappan Suresh, Takeshi Izumo
Funding acquisition: Iyyappan Suresh, Jérôme Vialard
Investigation: Iyyappan Suresh
Methodology: Iyyappan Suresh, Jérôme Vialard, Takeshi Izumo
Project administration: Iyyappan Suresh
Resources: Iyyappan Suresh
Software: Iyyappan Suresh
Supervision: Jérôme Vialard, Matthieu Lengaigne

1. Introduction

The subsurface oceanic variations along the west coast of India (WCI) have strong socio-economic and environmental impacts. Indeed, the thermocline depth variations are closely linked to the oxycline depth variations in this region (Parvathi et al., 2017). During boreal summer and fall, the upwelling brings the poorly oxygenated waters from the intense Oxygen Minimum Zone in the eastern Arabian Sea to the continental shelf off the WCI (e.g., Naqvi et al., 2006). This results in hypoxic or anoxic (i.e., oxygen-depleted) conditions along the coast, which can potentially inflict severe damage to the regional ecosystems and fisheries (Naqvi et al., 2009). As sea level is a good indicator of the thermocline and oxycline depth variations (Prakash et al., 2013), it is important to study its dynamics along the WCI.

Validation: Iyyappan Suresh
Visualization: Iyyappan Suresh, Matthieu Lengaigne
Writing – original draft: Iyyappan Suresh
Writing – review & editing: Iyyappan Suresh, Jérôme Vialard, Takeshi Izumo, Matthieu Lengaigne

Previous studies have focused on the dynamics of seasonal sea level (a proxy of thermocline depth) and currents variations along the WCI, or more generally, the dynamical response of the Northern Indian Ocean (NIO) to the seasonal reversal of monsoonal wind forcing (e.g., McCreary et al., 1993; Shankar & Shetye, 1997; Shankar et al., 2002). This dynamical response has been illustrated in a simple conceptual framework, called the "leaky waveguide," based on the equatorial linear wave theory (Shankar et al., 2002; Shetye, 1998). Winds blowing over the equatorial region force Kelvin waves (KW) that propagate eastward along the equator. A fraction of this incoming wave energy is reflected at the eastern boundary of the basin as westward-propagating equatorial Rossby waves (RW), while some of the energy propagates as coastal KWs through the coastal waveguides on either side of the equator. On the northern side, the coastal KWs propagate around the Bay of Bengal (BoB) rim, then around Sri Lanka, and northward along the WCI (McCreary et al., 1993). We will refer to this path of sea level signals as the BoB pathway (hereafter EQB; Figure 1a). The coastal waveguide is considered "leaky" on the eastern boundaries of the BoB and the Arabian Sea due to westward radiation of the coastal signals (Figure 1a) at periods longer than the RW minimum period (i.e., equatorward of a critical latitude for a given period). This framework has helped to highlight the prominent role of remote forcing in the NIO. McCreary et al. (1993) and Shankar et al. (2002), for example, demonstrated that a large part of the seasonal cycle of the West Indian Coastal Current (WICC) is driven by the wind variations over the BoB. Gopalakrishna et al. (2008) then suggested that the alongshore wind variations over the southern Sri Lankan coast may also play an important role for the observed sea level variability along the WCI. Using a linear continuously stratified (LCS) ocean model (McCreary et al., 1996; Suresh et al., 2013, 2016, 2018), Suresh et al. (2016) quantified that the wind forcing in a small region encompassing the southern tip of India and Sri Lanka (hereafter the STIP region, 75°E–90°E, 5–10°N, purple frame on Figure 1b) contributes ∼60% to the sea level seasonal cycle along the WCI. The variations of the wind-stress curl off the east coast of Sri Lanka and of the alongshore winds over the convoluted coastline in the STIP region force upwelling coastal KWs that propagate northward along the WCI, creating a "window of opportunity" for the occurrence of coastal anoxia by favoring shallow thermocline and thus oxycline depths during the late summer and fall seasons (Parvathi et al., 2017).

The interannual sea level variability along the WCI has received much less attention than that of the Bay of Bengal, due to its smaller amplitude. Parvathi et al. (2017) and Suresh et al. (2018) are to our knowledge the only studies that have addressed this topic in detail. The key role of the Indian Ocean Dipole (IOD; Murtugudde et al., 2000; Saji et al., 1999; Webster et al., 1999), the dominant mode of intrinsic climate variability in the Indian Ocean, on sea level and ocean heat content variations in the NIO has long been known (e.g., Currie et al., 2013; Yu et al., 2005). Parvathi et al. (2017) detailed the influence of IOD on sea level variations along the WCI, and highlighted its substantial socio-economic impacts through modulation of anoxic events. Sensitivity experiments performed by Suresh et al. (2018) using the LCS model further provided insights into the causes of these variations. They demonstrated that easterly wind anomalies in the STIP region during positive IOD events force coastal KWs, which induce downwelling and suppress anoxic events along the WCI. They also demonstrated that the "leaky" waveguide causes upwelling signals that slowly propagate as RWs through the interior BoB, resulting in a delayed upwelling signal during boreal winter along the WCI.

The main sources of atmospheric intraseasonal variability (ISV) over the Indian Ocean are the monsoon active-break phases during boreal summer (Goswami, 2005) and the Madden-Julian Oscillation (MJO) during winter (Zhang, 2005). Both of these phenomena induce wind variations. A recent study (Rohith et al., 2019) has identified a 1–2 cm amplitude barotropic sea level response to the MJO forcing. This response is nearly spatially homogeneous over the Indian Ocean, due to fast-propagating barotropic mode (phase speed ∼200 $m.s^{-1}$ in the deep ocean). Most of the studies have thus focused on the larger amplitude, spatially heterogenous baroclinic sea level response to ISV forcing that typically propagates at ∼2.5 $m.s^{-1}$ for the first baroclinic mode. The equatorial baroclinic response to the wind ISV has for instance been documented in numerous studies (e.g., Masumoto et al., 2005; Nagura & McPhaden, 2012; Sengupta et al., 2007). Using current measurements on the WCI and satellite altimeter observations, Vialard et al. (2009) showed that intraseasonal currents variations along the WCI are associated with basin-scale sea level ISV of the NIO. Using LCS model, Suresh et al. (2013) demonstrated that this basin-scale sea level response is primarily driven by wind forcing in the equatorial region, with signals propagating through the equatorial and coastal waveguides of the NIO. In particular, they estimated that equatorial wind signals contribute 60%–70% to the total sea level ISV along the WCI.

On the other hand, the winds over the STIP region exhibit large ISV (Figure 2a), both in the alongshore component (gray shading along the convoluted coastline) and in the wind-stress curl east of Sri Lanka (colored

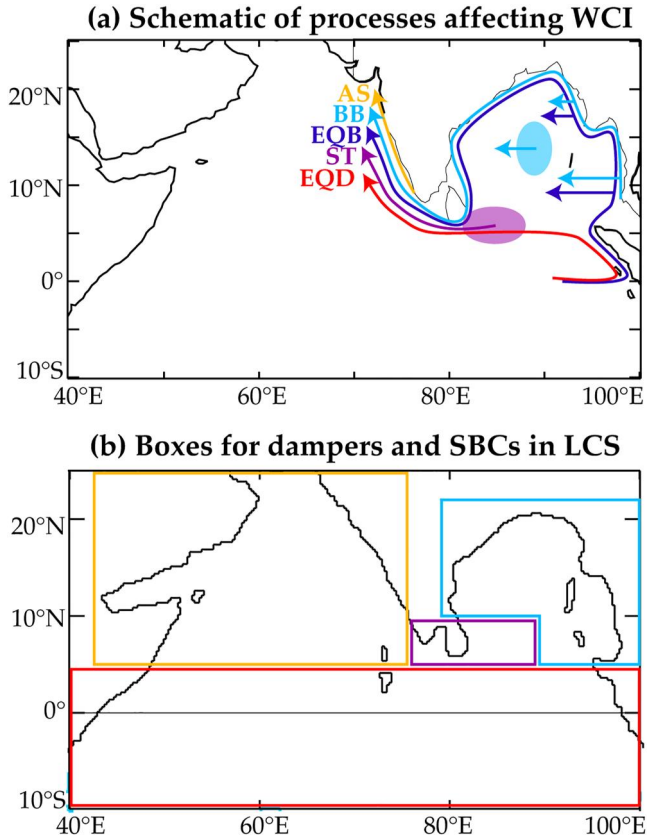

Figure 1. (a) Schematic representation of processes (pathways of signal propagation) that influence the sea level in the northern Indian Ocean, specifically off the West Coast of India (WCI). (b) The corresponding forcing regions (i.e., the boxes used for dampers and special boundary conditions (SBCs) indicated with matching colors in panel (a), with an exception that both dark blue and red signals originate in the red box), where the signals in panel a originate. The pathway of sea level signals originating in the equatorial Indian Ocean that propagate through the Bay of Bengal (BoB) coastal waveguide (EQB) is depicted in dark blue, while that propagate through the "direct connection" between the equatorial and coastal waveguides near Sri Lanka (EQD) is marked in red. The pathway of signals driven by the BoB forcing (BB; includes response to both alongshore forcing and wind-stress curl in the basin interior, symbolized with oval shading) is shown in light blue, while the propagation path of signals forced by winds near the southern tip of India and Sri Lanka is illustrated in purple (ST). The path of the coastal Kelvin wave forced by alongshore winds in the Arabian Sea (AS) are shown in orange. The arrows on the eastern BoB rim represents the "leaky" aspect of the coastal waveguide, that is, the westward radiation of signals as Rossby waves from the eastern rim of the BoB.

shading). The large wind-stress curl ISV in this low-latitude region drives strong Ekman pumping near Sri Lanka (Figure 2b). This strong forcing generates intraseasonal sea level signals that propagate to the WCI, and thus could contribute significantly to the WCI sea level ISV, possibly similarly to what has been demonstrated for the seasonal and interannual timescales (Suresh et al., 2016, 2018). Amol et al. (2012) indeed traced back intraseasonal current variations measured off the WCI to wind variations in this region. Similarly, Dhage and Strub (2016) found high correlations between the WCI intraseasonal sea level and STIP winds, also suggesting a significant role of intraseasonal wind forcing in this region. Our first objective will thus be to refine the results of Suresh et al. (2013) by quantifying the influence of wind variations in the STIP region on the WCI intraseasonal sea level.

An intriguing result of Suresh et al. (2013) study is that the contribution of equatorial signals to the sea level ISV is larger along the WCI (60%–70%) than along the East Coast of India (50%). This suggests the possibility of a direct connection between the equatorial waveguide and the WCI (red arrow on Figure 1a), in addition to the BoB pathway (Figure 1a). This possibility was ruled out in the initial "leaky waveguide" framework. The equatorial waveguide extends ∼250 km north of the equator. The coastal waveguide dominant e-folding scale is given by the first baroclinic Rossby radius of deformation, which is ∼200 km at the southern coast of Sri Lanka at 6°N (e.g., Chelton et al., 1998), leaving a gap of ∼100 km between the two waveguides (Shankar et al., 2002; Shetye, 1998). Shetye (1998) noted, however, that RWs can potentially excite coastal KW along the coast of Sri Lanka, but did not discuss this effect further in the context of WCI sea level variability. Figure 3 shows the sea level meridional structures of the first-baroclinic mode equatorial KW and first three meridional-mode equatorial RWs, computed using a KW phase speed of 2.5 $m.s^{-1}$ (e.g., Le Blanc & Boulanger, 2001). The red vertical line in Figure 3 marks the latitude of the southern tip of Sri Lanka. While equatorial KW has maximum amplitude at the equator and has only ∼15% of its peak amplitude at this latitude, the first three meridional RWs have a maximum amplitude at ∼3.5°, 5°, and 6.5°N, respectively, and are associated to much larger sea level perturbations along Sri Lankan coast that, in principle, can trigger coastal KWs. These theoretical arguments suggest that the equatorial and NIO coastal waveguides intersect at the southern tip of Sri Lanka, potentially setting up another pathway for the signals from the equator to the WCI. We will refer to this pathway of equatorial signals to the WCI as the "direct connection" or EQD (Figure 1a). Dhage and Strub (2016) is, to our knowledge, the only study that examined this hypothesis. Based on satellite measurements of sea level and winds, they suggested that "equatorial signals arriving through RWs from the east of Sri Lanka" exerted a more robust influence on the WCI intraseasonal sea level than signals propagating through the BoB pathway, concluding that "This result provides support for the result found in the modeling study by Suresh et al. (2013)." Their observational analysis did not quantify the relative importance of these two pathways. This will be our second objective.

In this paper, we aim at quantifying the major drivers of the WCI sea level ISV, including the local and remote forcing from (a) the equator through the BoB pathway (dark blue on Figure 1a); (b) the equator through the "direct" pathway (red); (c) the STIP region encompassing the southern tip of India/Sri Lanka (purple); (d) the rest of the BoB (light blue). To that end, we will run sensitivity experiments with the LCS ocean model, which enables us to cleanly separate the complete response into process solutions (McCreary et al., 1996), corresponding to each of the aforementioned forcing mechanism (see Section 3.2 and Supporting Information S1). The paper is organized as follows. In Section 2, we briefly describe our model and setup an idealized experiment that demonstrates

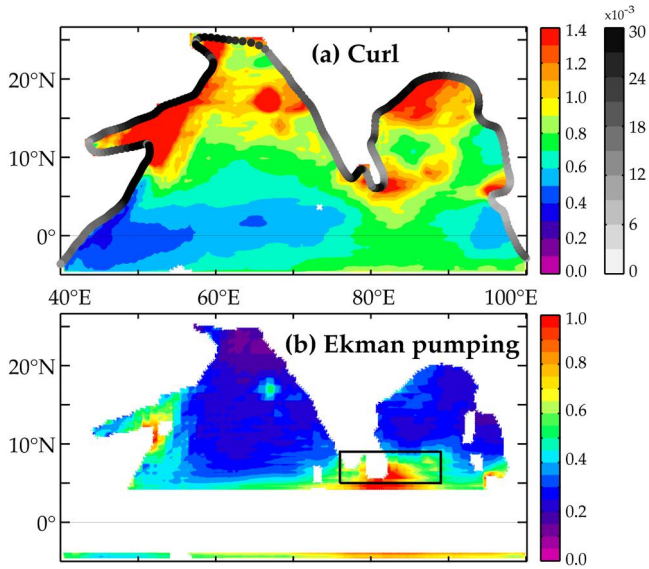

Figure 2. The standard deviation of intraseasonal (20–150 days) wind forcing (1984–2017 period). (a) Wind-stress curl ($\times 10^7$ N.m^{-3}, color shading) and alongshore wind stress ($\times 10^{-3}$ N.m^{-2}, gray shading along the coast). Note that their effects on oceanic transports are amplified equatorward by the 1/*f* factor. (b) Ekman pumping velocity (m.day^{-1}). The black frame marks the southern tip of India/Sri Lanka region (STIP; 75°E–90°E, 5–10°N) with strong intraseasonal wind variations.

the existence of the EQD pathway. In Section 3, we introduce the ocean model simulations with a realistic wind forcing, validate them for sea level ISV, and describe our methodology for quantifying the contributions from the above processes. In Section 4, we quantify the contributions of these processes to the NIO sea level ISV, specifically focusing on the WCI. In Section 5, we summarize our results and discuss them in the context of previous literature. We will in particular discuss why the "direct connection" that operates at the intraseasonal timescale is much weaker at longer timescales.

2. Intersecting Waveguides South of Sri Lanka: Idealized Experiments

We use a modified version of the linear, continuously stratified (LCS) ocean model of McCreary et al. (1996), which we have previously used for studying the NIO/WCI sea level dynamics at intraseasonal (Suresh et al., 2013), seasonal (Suresh et al., 2016) and interannual (Suresh et al., 2018) timescales. We focus here on sea level, known to be a good proxy of thermocline depth variations (see discussion on this approximation in Izumo & Colin, 2022). We provide a brief description of the model here (also the Supporting Information S1) and the reader can refer to the above articles for a more detailed description. The model solves the shallow water equations for the first 5 baroclinic modes, computed from the observed average Indian Ocean stratification. This solution does not include the barotropic mode described by Rohith et al. (2019). The model is run at ¼° resolution over the Indian Ocean (30°S–30°N, 30°E–110°E), with a coastline derived from 200-m isobaths. The model coastline is displayed on Figure 1b (note that the strait between India and Sri Lanka is less than 10 m deep at its shallowest point, and is thus closed in our model land-ocean configuration, as it does not allow baroclinic waves to pass through). As we will show in Section 3, the model reproduces the observed intraseasonal sea level variations in the NIO very well when forced with observed wind stresses.

As a proof of concept, we perform idealized experiments to illustrate the "EQD" connection in this section. First, the LCS model is forced with a westerly wind burst lasting for 10 days over a rectangular region extending from 87°E to 93°E and from 5°S to 5°N in the eastern equatorial Indian Ocean (see black vectors on Figure 4a). The geographical range for this wind patch has been chosen such that the sea level response to this forcing does not intersect and directly generate a signal at the Sri Lankan coast (such a signal would obscure the mechanism we want to highlight here). However, slight changes in the position of the wind patch do not affect our results. The forcing has a Gaussian shape symmetric about the equator in the meridional direction, with an arbitrary maximum wind-stress amplitude of 0.13 N.m^{-2}. In the zonal direction, the wind stress is constant and is linearly ramped down to zero within 1° from the eastern and western edges of the rectangular region. The wind stress is zero over the rest of the domain, and hence cannot directly force coastal KWs. We will refer to this idealized control experiment as ICTL.

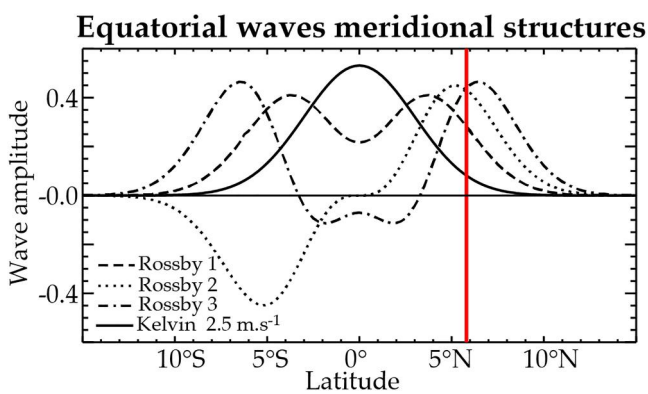

Figure 3. The sea level meridional structures (unitless) for first baroclinic mode (Kelvin wave phase speed of 2.5 m.s^{-1}) equatorial Kelvin wave and the first three Rossby waves meridional modes. The red vertical line marks the latitude (~6°N) of the southernmost coast of Sri Lanka.

As expected, the above idealized westerly wind forcing excites downwelling equatorial KWs to the east of the forcing region and upwelling equatorial RWs to the west (Figure 4a). When the eastward-traveling equatorial KW reaches the Sumatra coast, some of its energy is reflected back into the equatorial region as downwelling equatorial RWs, while some of its energy enters into the BoB coastal waveguide as downwelling coastal KWs (Figure 4b). While the downwelling signals through the BoB pathway have not yet reached the Sri Lanka region 20 days after the initiation, the signals associated with the forced upwelling RWs interact with the southern coast of Sri Lanka and set up upwelling coastal KWs that propagate along the WCI (Figure 4b). The ICTL experiment thus provides a first demonstration of the EQD pathway, associated with the RWs directly forced by the wind patch in

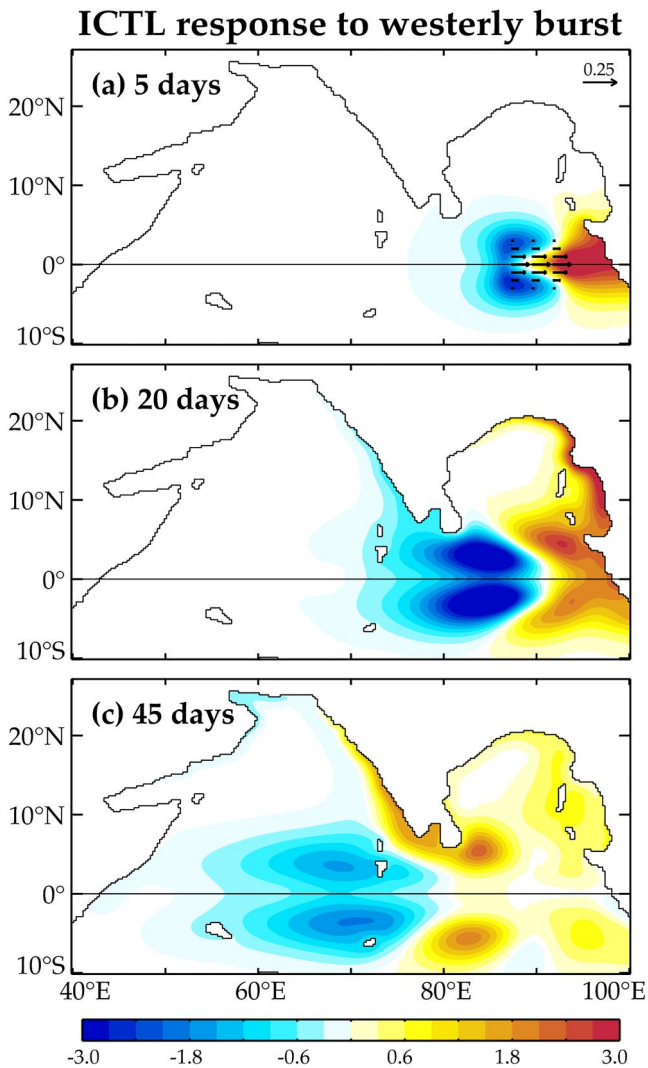

Figure 4. Snapshots of sea level anomalies (cm) from the ICTL experiment at (a) 5, (b) 20, and (c) 45 days after the initiation of a westerly wind-stress burst that lasts for 10 days. The wind stress patch is displayed as vectors (N. m^{-2}) in the eastern equatorial Indian Ocean in panel (a).

the equatorial band. At day 45 (Figure 4c), the downwelling RWs reflected at the eastern boundary of the basin and the downwelling coastal KWs via the "BoB" pathway reached the coast of Sri Lanka. The signal along the WCI at that time is thus a combination of the "direct" (EQD) and "BoB" (EQB) pathways. This idealized experiment thus clearly illustrates the EQD pathway, associated with both directly forced and reflected equatorial RWs.

While the first negative sea level anomaly on the WCI can be entirely attributed to the EQD pathway (Figure 4b), the later positive anomaly is a combination of signals from EQD and EQB pathways (Figure 4c). The distance from the Sumatra coast to the Sri Lankan east coast along the EQB pathway (~4,500 km along the coastal waveguide aligned to BoB rim) is about three times longer than that along the EQD pathway (~1,500 km from Sumatra coast directly to the east coast of Sri Lanka). As the EQB signals (coastal KW) travel three times faster than the EQD signals (first-meridional mode equatorial RW), it takes nearly the same amount of time for the reflected RW and the coastal KW from Sumatra coast to reach the east coast of Sri Lanka, making it difficult to separate these signals. However, the two processes can be isolated based on an additional LCS model experiment with a Newtonian damper (McCreary et al., 1996) over the BoB (applied within the dashed frame on Figure 5). In this experiment, the damper annihilates the signals transiting through the BoB (i.e., the EQB) and only retains those resulting from the EQD pathway. Since the model is linear, the EQB signal can be obtained as the difference between the ICTL and the above experiment. The reader is referred to Suresh et al. (2016, 2018) for a more complete description of similar sensitivity experiments with the LCS model.

Figures 5a–5d shows the results of the above decomposition. Figure 5d shows sea level time series at one location on the WCI (black box on Figures 5a–5c), referred to as total sea level, and its decomposition into EQD and EQB signals. As mentioned above, the first negative sea level signal on the WCI (peaking at ~25 days) is entirely associated with the EQD pathway due to interaction of the forced upwelling RWs with Sri Lanka that sets up coastal KWs. The sea level on the WCI turns to positive after 35 days and peaks at ~50 days, in association with the near simultaneous arrival of the downwelling signals from the EQD and EQB pathways (Figure 5d). Figures 5a–5c show snapshots of the total, EQD and EQB sea levels at the time when WCI sea level peak, that is, ~50 days after the wind burst initiation. At this time, sea level at the WCI is dominated by EQD, whose contribution to the first positive lobe at the WCI is about twice that of EQB (Figures 5b and 5d). The strongest signal at the WCI occurs ~50 days after the wind burst initiation. Weaker signals occur later both for EQD (reflections, higher order meridional mode RWs) and EQB (signals transiting through the southern BoB interior as RWs), but we will not discuss them further.

The presence of the Sri Lankan landmass is crucial for an effective EQD connection. This is demonstrated with an additional set of idealized experiments. The first idealized sensitivity experiment is as ICTL, but with a modified coastline in which the Sri Lankan landmass is removed (hereafter INOSL experiment). The corresponding snapshots and the sea level time series are displayed in Figures 5e–5h. The main effect of removing Sri Lanka is to reduce the EQD contribution to WCI, because the reflected RW amplitudes have a smaller contribution at the southern tip of India (around 8°N) than at the coast of Sri Lanka (around 6°N, see Figure 3), resulting in a EQD contribution roughly reduced by half compared to ICTL (Figure 5d vs. Figure 5h). The second effect of removing Sri Lanka is that the EQB pathway to the WCI is now shorter, and the EQB downwelling wave reaches the WCI a couple of days before that of EQD (Figure 5h). The amplitude of EQB is slightly larger than that in the ICTL due to the shorter pathway length of the coastal KW when Sri Lanka is removed, and hence reduced travel time and frictional damping. A similar experiment in which both Sri Lanka and Indian landmass south of 10°S are removed

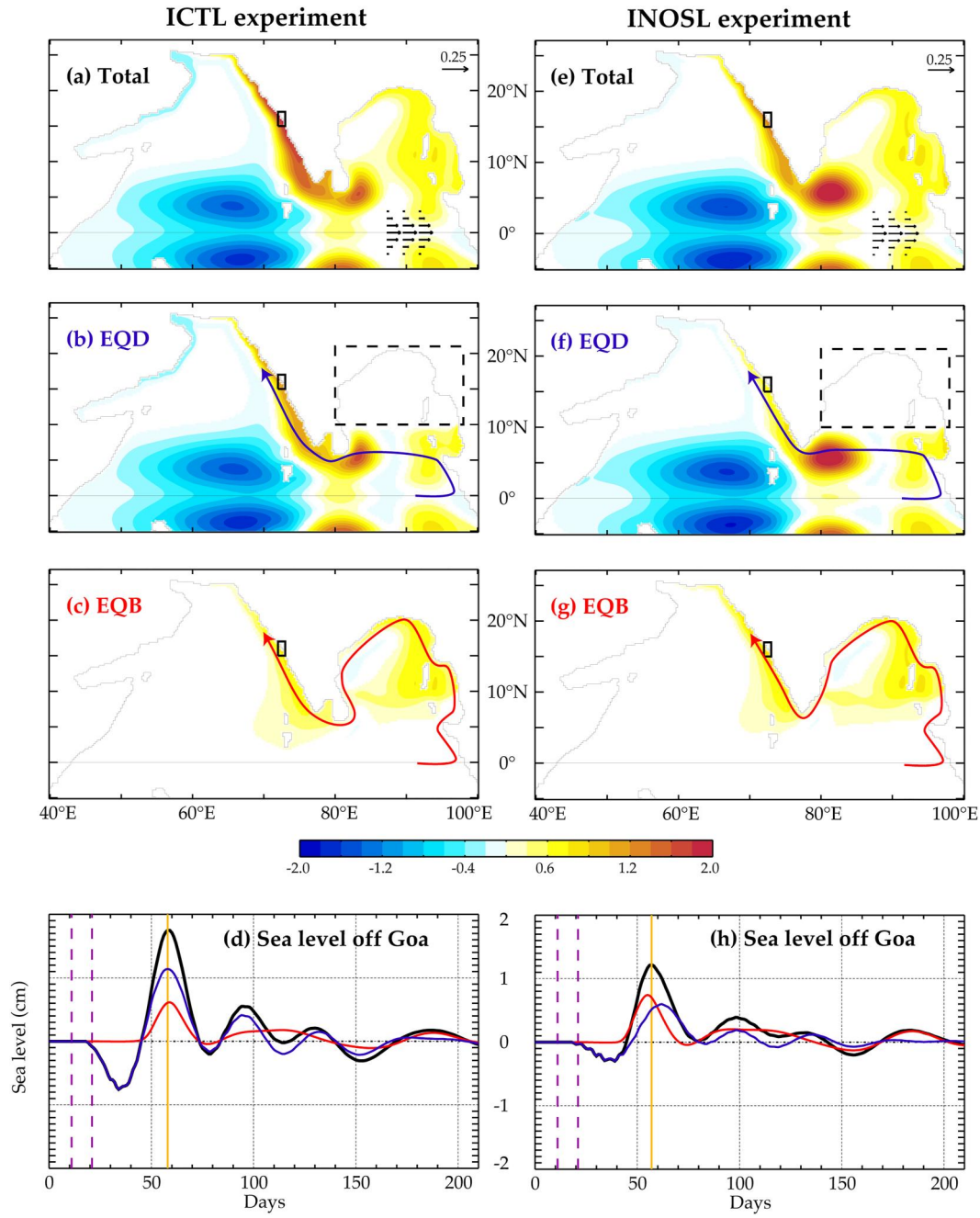

Figure 5. Snapshots of sea level (cm, color shading) patterns at the time of the maximum sea level anomaly in the black frame along the West Coast of India (WCI) in idealized LCS experiments with a short-lived localized westerly wind burst (vectors on panels a and e, $N.m^{-2}$) applied at days 0–10 (shading on panels d–h). The left panels (a)–(d) correspond to the idealized run with the original model coastline (ICTL) and the right panels (e)–(h) to the run without Sri Lanka (INOSL). The first row (a, e) shows the total sea level anomaly, the second (b, f) the contribution from the direct "EQD" connection and the third (c, g) that from the EQB (equatorial signals through BoB) contributions (see Figure 1). The bottom panels show time series of the total (black), EQD (red) and EQB (dark blue) contributions in the WCI box (black frame on maps). The yellow vertical line on the bottom panel time series indicates the timing of the snapshots above. The dashed black frames on the second row indicate the damper that is applied to separate the EQD and EQB processes (see Section 2 in text). The schematic arrows on (b, c, f, g) indicate the propagation pathways associated with the EQD (red) and EQB (blue) processes.

results in almost no contribution from the EQD pathway (not shown), as expected. Another experiment indicates that the presence of the Maldives islands does not affect the EQD pathway (not shown).

Although the above set of idealized experiments clearly demonstrates the potential importance of the EQD pathway for the WCI sea level variability, many caveats remain. The amplitude of the EQD signal on WCI depends on the choice of wind forcing. Shifting the wind forcing toward the western equatorial Indian Ocean results in a nearly equal or slightly weaker amplitude of EQD relative to EQB (not shown). In contrast, increasing the meridional length scale of the forcing in ICTL experiment increases the amplitude of the initial signal at the WCI, because higher-order meridional modes are excited (not shown). Finally, some studies have reported that basin resonances within the Indian Ocean favor intraseasonal periods around 90 days (Han, 2005; Han et al., 2011). Here we have simply explored the NIO's response to a single 10-day long wind pulse, rather than the response to an oscillatory forcing, knowing that this oscillating response can be mathematically retrieved from the impulse response through a simple convolution, thanks to model's linearity (cf. Section 4.3). While the above idealized experiments clearly indicate that its existence, we need to isolate the EQD process and quantify its contribution in the model experiments with realistic wind-stress forcing over the Indian Ocean.

3. Experiments With Realistic Wind Forcing: Methods and Validation

In this section, we will briefly describe our model experiments with realistic forcing, validate its intraseasonal sea level variations against satellite altimetry data (Section 3.1), and describe our method for decomposing the sea level variations into various processes (Section 3.2).

3.1. The Control Experiment and Its Validation

The LCS model described in Section 2 (with its realistic coastline) is forced with daily TropFlux (Praveen Kumar et al., 2013) wind-stress (available from http://www.incois.gov.in/tropflux/) anomalies (long-term mean removed) over the 1979–2018 period. This simulation is referred to as the control (CTL) experiment. The solution retains the first 5 baroclinic modes. The first baroclinic mode contributes to more than 90% of the variability in the NIO coastal waveguide, and more than 70% in the equatorial waveguide (the second baroclinic mode contributes to less than 10% in the coastal waveguide, but 20%–30% along the equator; the higher order modes contribute to less than 5% along the entire NIO waveguide; not shown).

We use the Ssalto/Duacs Sea Level Anomaly product on a ¼° grid, obtained from merging the altimeter data from various satellite missions (details, including download links, available on http://www.aviso.altimetry.fr/duacs/) and distributed by the Copernicus Marine Environment Monitoring Service (CMEMS), to validate our model. This data set is interpolated to the model grid. The observed and modeled intraseasonal sea levels are obtained as follows. The long-term linear trend and the seasonal cycle (based on the fit on the first four harmonics of the annual cycle) are first removed. The resulting anomalies are band-pass filtered in the 20–150–day window, based on a Fourier transform. The results of this study are not sensitive to the choice of a less selective (e.g., Hanning) filter or different choices of the filtering bandwidth such as 30–70 or 70–110 days (not shown).

The large-scale intraseasonal sea level patterns in the observations and CTL simulation are obtained using an empirical orthogonal function (EOF) analysis of the intraseasonal sea level, as in Suresh et al. (2013). We chose this EOF approach instead of point-wise validation as the observed sea level is influenced significantly by non-linearities, particularly in the eddy-rich regions of Bay of Bengal and Arabian Sea (Chen et al., 2012; Cui et al., 2016). Unlike observations, the LCS model does not produce eddies. We rely on the EOF method to extract the basin-scale response to wind forcing, and separate it from the much smaller-scale eddy effects. Furthermore, as noted in Section 2, the LCS model neglects the barotropic variability. However, observations include both the baroclinic response of our interest and the barotropic response discussed by Rohith et al. (2019). Since the latter response is spatially homogeneous over the Indian Ocean, it is eliminated by removing the domain average prior to performing the EOF analysis. Due to the strong meso-scale eddy activity in the western AS in observations, the EOF domain is restricted to the 55°E–100°E, 5°S–25°N region. The first EOF is well separated from higher-order EOFs in both model and observations. The first EOF (EOF1) explains 44% of the total variance in the model, but only 24% in observations. This is again because our linear model does not produce mesoscale eddies, which are energetic in observations, in particular in the northwestern BoB (e.g., Chen et al., 2012; Cui et al., 2016). The lagged auto-correlations of first Principal Component (PC1) indicates that the EOF1 dominant timescale is about

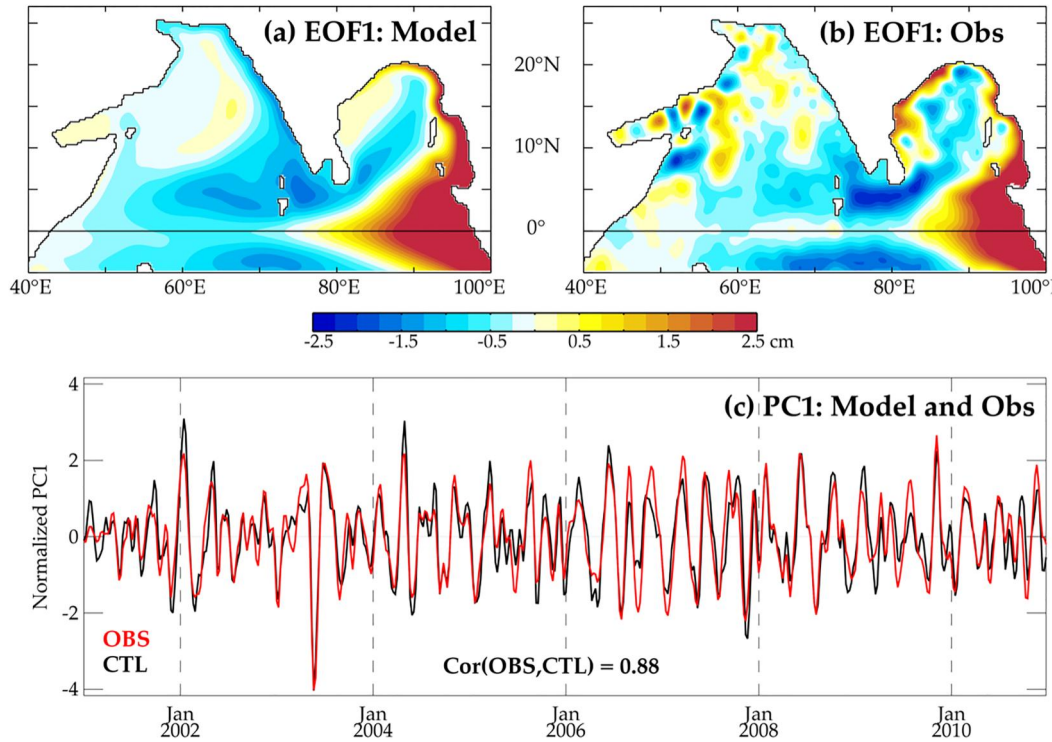

Figure 6. The dominant pattern of baroclinic intraseasonal sea level variability in (a) model control (CTL) experiment and (b) observations (Ssalto/Duacs merged sea level anomalies described in Section 3). To obtain the dominant pattern, we first perform empirical orthogonal function (EOF) analysis of the 20–150 days filtered sea level anomalies, relative to the climatological seasonal cycle, over the [55°E–100°E, 5°S–25°N] region. The associated sea level (shading; cm) patterns over the entire north Indian Ocean were then obtained through regression on to their respective normalized modeled (black) and observed (red) first Principal Components (PC1s) displayed on panel (c). The spatial pattern correlation between the modeled and observed EOF1s is 0.91 and the correlation between their PC1s is 0.88.

~90 days in the model and observations (not shown), in relation with the resonance mechanism emphasized by Han (2005).

Figures 6a and 6b show that the spatial pattern of EOF1 of the baroclinic intraseasonal sea level are very similar in the model and observations (0.91 pattern correlation), despite a slight amplitude underestimation in the model. These intraseasonal sea level patterns are remarkably similar to those in Suresh et al. (2013) (their Figures 1b and 1f), although they use a different wind-stress product (QuikSCAT) to force their model, and also to those shown by Vialard et al. (2009) for observations (their Figure 3), though they used a different method of analysis. This suggests that these large-scale intraseasonal sea level patterns are robust and essentially reveal the same underlying dynamics. With a 0.88 correlation, the modeled sea level PC1 further displays a very good phase agreement with that from observations (Figure 6c). Overall, the model reproduces observed intraseasonal sea level fluctuations in the NIO equatorial and coastal waveguides very well, both in terms of spatial pattern and phase agreement with observations. We will describe the full cycle of intraseasonal wind forcing and the dynamics of the associated sea level response in Section 4.

3.2. Methodology to Obtain Processes Contributions

We use a suite of LCS model experiments to decompose the NIO sea level into signals resulting from various processes shown on Figure 1a and listed below:

- *EQD*: sea level response to the equatorial wind forcing that follows the "direct" pathway to the WCI, resulting from the interaction of forced or reflected equatorial RWs with Sri Lanka and the tip of India, demonstrated in Section 2. By construction, we retain sea level in the equatorial band in EQD rather than in EQB process.

- *EQB*: sea level response to the equatorial wind forcing that follows the "BoB" "leaky" waveguide, that is, that follows the BoB rim as coastal KWs and that transits through the BoB interior as RWs.
- *ST*: sea level response to the alongshore wind and interior wind-stress curl forcing within the STIP region, a hotspot of intraseasonal wind forcing (Figure 1b) discussed in the introduction.
- *BB*: sea level response to the alongshore wind and interior wind-stress curl forcing over the remainder of the BoB (i.e., excluding the "STIP" region, Figure 1b);
- *AS*: sea level response to the alongshore wind and interior wind-stress curl forcing over the Arabian Sea.

Note that we have retained the sea level response to wind forcing over the southern hemisphere (i.e., south of the equatorial band) in the EQB and EQD processes. The southern hemisphere wind forcing can indeed excite signals that travel to the western boundary as RWs, turn to the equator as coastal KWs and then along the equator as KWs, and thus can contribute to NIO sea level in the same way as the signals originating at the equator. However, a separate experiment (by applying a damper south of 10°S; not shown) demonstrated that this contribution is quite small, consistent with Suresh et al. (2013), and that equatorial signals are largely forced by wind variations within the 5°N–5°S (equatorial) band.

The general principle of the methodology that allows the above process decomposition is similar to that in Suresh et al. (2016, 2018), or to the experiments discussed in Section 2, and is detailed in Supporting Information S1. A series of experiments with Newtonian dampers incrementally added in various regions (Figure 1b) allows isolating individual processes in the list above, and each contribution is then obtained using the linearity of our model. Note that we also used special lateral boundary conditions (SBCs) introduced by McCreary et al. (1993) to further decompose ST, BoB, and AS processes into contributions from alongshore and interior wind forcing, as was done in Suresh et al. (2018), but found that those details do not add much insights to the results reported here. By design of our methodology and linearity of our model, the sum of the above process solutions is equal to the CTL solution (verified that it is the case).

4. Experiments With Realistic Wind Forcing: Results

In this section, we will first discuss the basin scale patterns of the sea level ISV, and the main processes that contribute to this pattern. We will then more specifically discuss contributions from all the processes at specific coastal locations representative of eastern and western BoB and the WCI. Finally, we will investigate if the "EQD" pathway to the WCI is also active at seasonal and interannual timescales, and the reasons thereof.

4.1. Process Decomposition of Basin Scale Intraseasonal Sea Level Patterns

Figures 7a–7c display the modeled basin-scale intraseasonal sea level and wind-stress patterns obtained from a lead/lag regression to the intraseasonal sea level PC1 (Figure 6c). The large-scale sea level patterns at lags −14 (Figure 7a) and 28 days (not shown) are almost the same but with opposite polarity, confirming that the dominant timescale of sea level intraseasonal variations is about 90 days (Han, 2005). The westerly wind anomalies at lag −14 (Figure 7a) exhibit maximum over the central and eastern equatorial Indian Ocean, and have a broad meridional scale (up to ∼10°N). They are related to the active phase of the MJO or intraseasonal oscillations in the east Indian Ocean, with increased precipitation there (Zhang, 2005). These wind anomalies force downwelling equatorial KWs to the east and upwelling equatorial RWs to the west. These RWs interact with Sri Lanka and the southern tip of India (Figure 7a), thus establishing the EQD pathway. It is difficult to distinguish those upwelling RWs from the response to the local forcing in the vicinity of Sri Lanka, where the cyclonic wind stress (positive wind-stress curl) is also favorable to upwelling (Figure 7a). The downwelling KW reflection at the eastern boundary is associated with downwelling coastal KWs that propagate into the BoB waveguide (Figures 7b and 7c) and with reflected downwelling equatorial RWs that are clearly visible in Figure 7c (centered ∼5°N). Those reflected RWs have meridional modes 1–3 contributions, as suggested by a broad (5–8°N) maximum, including a mode 2 asymmetrical component relative to the equator. The downwelling signals through the EQD and EQB pathways merge near Sri Lanka around lag 14 days (Figure 7c), inducing coastal KW signals that propagate to the WCI afterward.

Figure 7 displays the ST (d–f), EQB (g–i), and EQD (j–l) processes. The BB and AS processes contribute only weakly to the WCI sea level ISV and hence are not shown (see Section 4.2). The AS process is limited to the effect of alongshore wind stress on the WCI. The alongshore wind stress components tend to be weak along the WCI (Figure 1b shows the forcing region for AS), except within the STIP region (Figures 7a and 7c). The BB

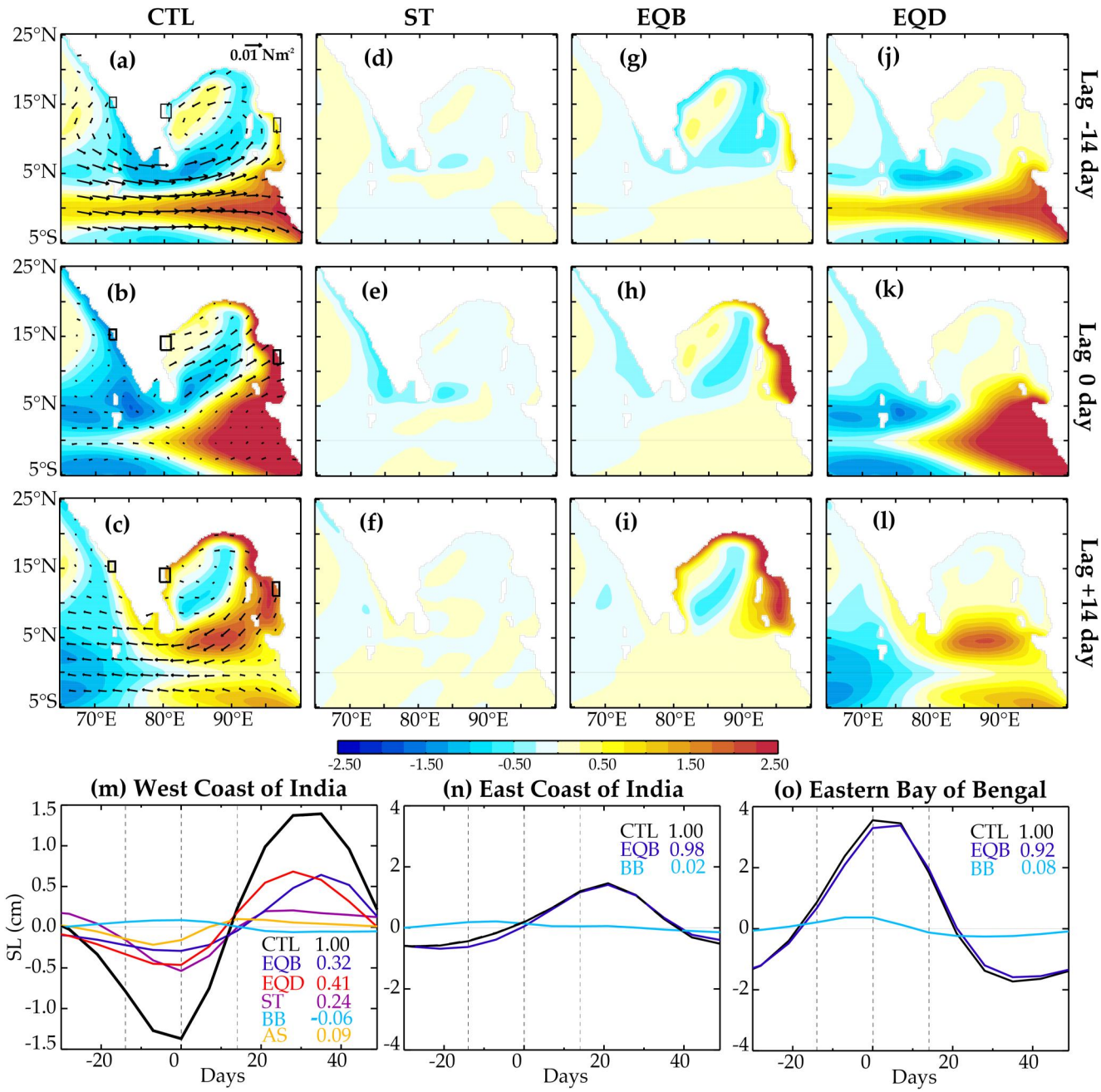

Figure 7. Lag-regression (lags are indicated on the right) maps to the normalized principal component (shown in Figure 6c; multiplied by −1) of the EOF1 of CTL intraseasonal sea level. (a–c) CTL intraseasonal wind stress forcing (vectors, $N.m^{-2}$) and sea level response (shading, cm, color bar below) and its contributions from the (d–f) ST, (g–i) EQB process, and the (j–l) EQD processes. The maps for BB and AS contributions have been omitted as they have a much smaller amplitude, but they are displayed on the time series of panels (m)–(o). Typical intraseasonal coastal sea level (cm) variations at (m) the west coast of India (72–73°E; 14.5–16°N, boxes on panels a–c), (n) the east coast of India (79.5–81°E, 13–15°N) and (o) in the eastern BoB rim (96–97°E; 11–13°N), and contributions from the processes described on Figure 1. Those have been obtained from the lead/lag regression of the total sea level and its components at each coastal location to the normalized CTL PC1, shown on Figure 6c. The dashed vertical lines indicate the lags at which the sea level patterns are displayed on panels (a–l). The numbers next to the process labels indicate the regression coefficient of each process to the total CTL sea level.

contribution is also quite weak along the WCI, probably because of the corresponding wind pattern (shown in Figures 7a–7c) that reverses in BoB in a ∼30 days timescale. This can result in a negative interference for the slowly propagating RWs induced by those winds in the BoB interior. We will further discuss those two processes in Section 4.2.

Isolating the EQD process allows visualizing the direct connection between the equatorial band and the WCI, that is, how equatorial RWs (forced/reflected) interact with Sri Lanka and the southern tip of India and how signals propagate to the WCI (Figures 7j–7l). The downwelling signals reflected at the eastern boundary take about 4 weeks to propagate from Sumatra to the Sri Lankan east coast (Figures 7j and 7l from lags −14 to 14), which is consistent with the phase speed of the first baroclinic first meridional mode (50 ± 10 cm.s^{-1}) estimated by Webber et al. (2012) or Dhage and Strub (2016). These signals then propagate as coastal KWs along the WCI (Figure 7l). We will confirm in the next section that the EQD pathway yields larger sea level intraseasonal anomalies at the WCI than the ST and EQB processes.

The EQB pathway isolated in our experiments (Figures 7g–7i) is consistent with the "leaky waveguide" conceptual framework (Shankar et al., 2002). The sea level intraseasonal signals propagate rapidly (∼2.5 m.s^{-1}) along the BoB rim as coastal KWs (Figures 7g–7i). These signals also propagate westward through the interior BoB as RWs: see the J-shaped (a result of faster propagation of RWs at lower latitudes) negative sea level patch that slowly propagates westward on Figures 7g–7i. This westward radiation of RWs appears to occur over the entire eastern BoB rim (up to 19°N). The minimum period for first baroclinic mode RWs is about 95 days at 15°N (Suresh et al., 2013; Vialard et al., 2009). This implies that while the dominant timescale of the intraseasonal signal described here is 90 days, it also has energy at lower frequencies, which allow this offshore propagation over entire latitudinal range of the BoB. Because of this low-frequency component, Figure 7g shows a wave number-2 zonal pattern in the BoB interior, that is, signals from the current (negative) and previous (positive) oscillations. The opposite phase signal (positive) from the previous oscillation tends to attenuate the opposite signal (negative) that reaches the east coast of India after having traveled through the BoB coastal waveguide (e.g., Figure 7g). This destructive interference between coastal and offshore signals along the western BoB rim weakens the EQB amplitude there and, consequently, along the Sri Lankan coast and the WCI.

As expected, the strong cyclonic alongshore signal and the positive wind-stress curl in the STIP region at lag −14 (Figure 7a) force upwelling signals that propagate rapidly along the WCI as coastal KWs (Figures 7d and 7e).

4.2. Quantifying the Process Contributions at Representative Coastal Locations

We will now quantify the contributions from all the processes to intraseasonal sea level at specific locations (marked on Figures 7a–7c) along the BoB coastal waveguide and the WCI. The findings presented from those locations serve as representative indicators of the corresponding coastal sea level dynamics, as the results are robust for other choices.

The CTL offshore sea level ISV in the western and eastern BoB is almost entirely due to EQB signals (the regression coefficient of EQB to the CTL sea levels are more than 0.9 along both the coasts; Figures 7n and 7o). The dominance of EQB on intraseasonal sea level along the BoB waveguide is consistent with the results of Suresh et al. (2013), and similar to that at seasonal sea level (McCreary et al., 1996; Shankar et al., 1996). The EQB and the total sea levels in the western BoB (east coast of India) are nearly half of those in the eastern BoB (Figure 7n vs. Figure 7o), probably due to a combination of Newtonian dissipation of the signal along its pathway and the destructive interference with the opposite phase signals from the previous oscillation that has traveled as RWs (radiated by EQB signals at the eastern BoB rim) through the interior BoB, as discussed in Section 4.1 (Figure 7g). The EQB signal at the east coast of India lags that at eastern BoB by ∼20 days (compare the peaks in Figures 7n and 7o), which corresponds to propagation time of first baroclinic mode KW along the BoB coastal waveguide. The local wind forcing contribution (BB process) is weak in the BoB (the regression coefficient of BB to the CTL sea level is 0.08 in the eastern BoB, and much weaker on the east coast of India). This small BB contribution corresponds to alongshore wind forcing: the winds indeed have northward/southward (southeastern/northwester BOB rim) alongshore components at lags −14 and +14 days (Figures 7a and 7c), inducing upwelling/downwelling coastal signals.

The WCI sea level is also influenced by EQD, ST, and AS processes in addition to those processes affecting the BoB (Figure 1a). The WCI EQB signal lags behind that at the east coast of India by ∼14 days (Figures 7m and 7n), which corresponds to the time for first baroclinic mode coastal KW to travel around Sri Lanka and to reach the WCI (at 15°N). The regression coefficient of EQB to the total variability is 0.32 (Figure 7m). The EQD process, however, has a stronger contribution to the WCI, with a regression coefficient of 0.41 (Figure 7m). Although the EQD is almost in phase with the EQB as explained in Section 2, there is still a ∼7 days lead (Figure 7m) as illustrated in Figures 7i and 7l (at lag +14 days, the EQD RWs are already interacting with the STIP, while the

EQB coastal KWs have not yet reached Sri Lanka). Both EQD and EQB have their largest contributions to the WCI at positive lags of ∼25 and ∼35 days respectively (Figure 7m), as the sea level response to the strong wind forcing (equatorial westerlies at lag −14 days) takes about ∼40 and ∼50 days to reach the WCI (∼50 days in the idealized experiment with Gaussian wind pulse shown in Figure 5d). The third dominant contribution to the WCI sea level ISV is ST (its regression coefficient to the total sea level ISV is 0.24), and this contribution is stronger at negative than at positive lags (magenta curve on Figure 7m). This can particularly be attributed to the strong alongshore wind and wind-stress curl forcing at lag −14 days (Figure 7a), whose response rapidly propagates to the WCI (Figures 7d and 7e). The AS process narrows down to the alongshore wind forcing for the WCI box. Though in phase, it has only a weak contribution to the total intraseasonal sea level (with a 0.09 regression coefficient). This contribution is evident for negative lags, in relation with the southward alongshore wind-stress component along southern part of the WCI that excites upwelling KWs at lag −14 days (Figure 7a). The BB contribution to the WCI is the weakest and is in phase opposition with the total signal (regression coefficient of −0.06). This can be explained by the tendency of alongshore and interior wind forcing in the BoB to generate sea level signals, which are out of phase with each other. For instance, the cyclonic wind-stress curl in BoB at lag −14 days is favorable to open-ocean upwelling, while the southward alongshore winds over the northwestern BoB rim is favorable to downwelling (Figure 7a). Those two signals interfere destructively, resulting in overall weakening of BB signals. While the BB and AS contributions to WCI sea level ISV are weak on annual average, those forcing could become stronger during summer due to the northward shift of the wind anomalies, as previously discussed by Suresh et al. (2013) (see their Figure 3).

Overall, we find that the intraseasonal coastal sea level signals in the BoB behave as expected from the "leaky waveguide" conceptual framework, with a dominant contribution from the equatorial forcing through the BoB pathway, which includes both coastal KWs and interior RWs radiated from BoB eastern boundary, and weak contribution from the BoB wind forcing at the intraseasonal timescale. Over the WCI, however, our study confirms two previous hypotheses. First, the equatorial RWs, either forced or reflected at the equatorial eastern boundary, interact with Sri Lanka and establish a new direct pathway from the equator to the WCI, as previously suggested by Suresh et al. (2013) and Dhage and Strub (2016), but not described within the "leaky waveguide" concept. We further quantified that this EQD pathway is the main contributor to the intraseasonal sea level variations on the WCI. Second, we confirm that intraseasonal wind variations near the southern tip of India and Sri Lanka (STIP region) contribute to the WCI intraseasonal sea level variations, as previously suggested by Amol et al. (2012) and Dhage and Strub (2016), although this contribution is weaker than that of the EQD and EQB processes.

4.3. The EQD Connection at Seasonal and Interannual Timescales

In this subsection, we investigate if the EQD connection, which is the dominant process for the WCI sea level ISV, does operate efficiently at seasonal and interannual timescales. To that end, we use the same sets of realistic simulations discussed in Sections 3 and 4 and the same methodology to decompose the seasonal and interannual sea level signals into their various contributing processes. The seasonal cycle is obtained from a fit to the first four harmonics of the annual cycle and the interannual anomalies are obtained by subjecting the detrended anomalies relative to the above seasonal cycle through a bandpass filter in the 150-day to 7-year window.

Figure 8a displays the mean seasonal cycle of sea level on the WCI and its underlying process contributions. Figure 8a is remarkably similar to Figure 2b in Suresh et al. (2016), except that the sea level due to remote equatorial forcing is further decomposed into EQD and EQB. Both contributions (0.1 and −0.06 regression coefficients for EQD and EQB, respectively) to the total sea level seasonal cycle are small. Figure 8a illustrates that the EQB and EQD signals tend to be in opposite phase, explaining the overall weak equatorial contribution to the WCI, as demonstrated previously by Suresh et al. (2016). The bottom line is that the EQD pathway does not operate effectively at the seasonal timescale and it is four times weaker than that at the intraseasonal timescale (cf. discussion below). Let us now examine EQD at the interannual timescale.

As discussed in the introduction, IOD is the main mode of Indian Ocean climate variability affecting the interannual sea level variations on the WCI (Suresh et al., 2018). Figure 8b displays the IOD-induced sea level anomalies on the WCI and its components resulting from various processes, obtained in the same way as in Suresh et al. (2018) (their Figure 3) by (lead/lag) regressing the respective (total and individual processes) sea level on to the normalized September–November average Dipole Mode Index (Saji et al., 1999), downloaded from https://psl.noaa.gov/gcos_wgsp/Timeseries/Data/dmi.had.long.data. Figure 8b is strikingly similar to Figure 3a in

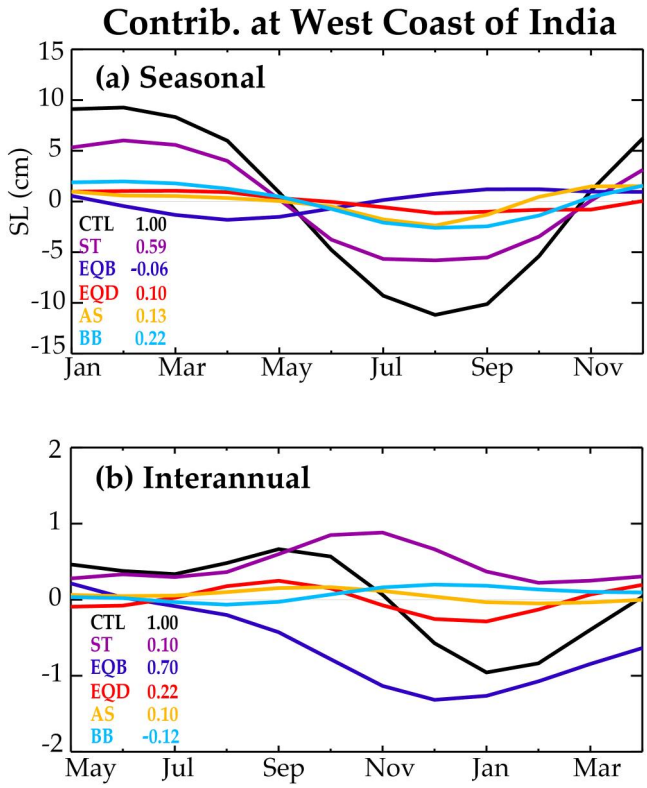

Figure 8. West coast of India sea level (cm) and contributions from various processes. (a) Mean seasonal cycle; (b) typical interannual sea level anomalies associated with a positive Indian Ocean Dipole (IOD) event, obtained as the lead-lag regression to the average September–November Dipole Mode Index. The color code is the same as that in Figure 7m. The numbers next to the process labels indicate the regression coefficient of each process sea level to the total CTL sea level.

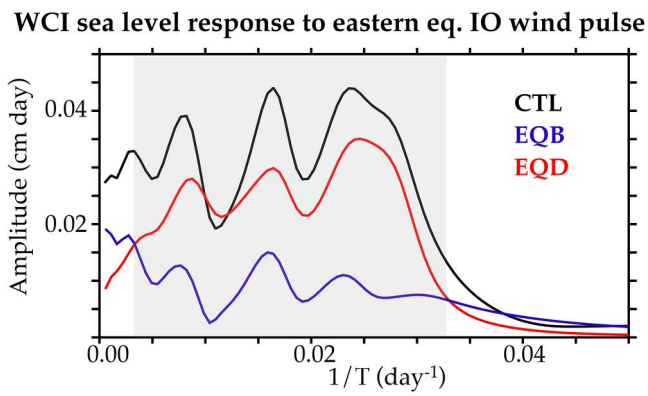

Figure 9. Frequency-response (cm.day) diagram of the sea level signal along the west coast of India (black) and its contributions from the direct connection at the southern tip of Sri Lanka (EQD, red) and the signals transiting through the Bay of Bengal (EQB, blue), to an equatorial wind patch in the eastern Indian Ocean (see Figure 4a for the wind patch spatial pattern). This frequency-response was obtained from the Fourier transform of the sea level response (shown in Figure 5d) along the west coast of India, in the impulse experiments displayed on Figures 4 and 5a–5d. The gray shading indicates the 30–280 days band, for which the amplitude of the EQD contribution to west coast of India sea level is larger than that of EQB.

Suresh et al. (2018), but shows decomposition of sea level due to remote equatorial forcing into EQD and EQB signals. Consistent with Suresh et al. (2018); Figure 8b indicates that the main contributor to the WCI downwelling (positive) signal during positive IOD events is ST process, that is, the wind forcing in the STIP region. The delayed opposite (negative, upwelling) signal on the WCI during the following winter is almost entirely due to the slowly propagating RWs through the BoB interior (included in EQB process, with 0.7 regression), as described in Suresh et al. (2018). The EQD however has a slight contribution to the delayed upwelling signal (Figure 8b), but it is roughly three times smaller than that of the EQB signal (regressions to the total signal of 0.7 and 0.22, respectively; Figure 8b). The EQD pathway is twice weaker at the interannual (0.22) than at the intraseasonal (0.41) timescale.

The question remains to be answered is: why is the EQD signal much weaker at the seasonal and interannual timescales than at the intraseasonal timescale? We first note at the seasonal timescale that the zonal wind-stress variations along the equator are weaker than the monsoonal wind-stress variations in the NIO. Suresh et al. (2016) for instance report typical alongshore seasonal wind-stress amplitudes above 0.06 $N.m^{-2}$ (their Figure 1b), while the amplitude of the zonal wind-stress seasonal cycle at the equator is <0.03 $N.m^{-2}$ (Schott & McCreary, 2001; their Figure 3). Next, we note that the equatorial Indian Ocean exhibits basin resonance at ~90 days, highlighted by Han (2005), that involves strong RW amplitudes in the eastern basin, specifically in the STIP region (e.g., Figure 13 of Han et al., 2011). One reason for this resonance is that the wind forcing reverses south of India from westerlies at ~lag −14 days (Figure 7a) to easterlies at ~lag +28 days (not shown; but can be seen in Figure 7c), which corresponds to the time it takes for the forced downwelling KW on Figure 7a (−14-day lag) to reach the eastern boundary and the reflected downwelling RW to reach the initial forcing region (+28-day lag). This reflected sea level signal is further reinforced by the signals due to local equatorial wind forcing (easterlies), as discussed in Sengupta et al. (2007), resulting in a strong ~90-day resonant oscillation. Figure 9 shows the frequency-response diagram of the WCI sea level from the idealized experiment (ICTL) forced with wind pulse (show in Figure 4a) in the equatorial eastern Indian Ocean, described in Section 2, and its decomposition into EQB and EQD processes. Due to the linearity of our LCS model, this frequency-response is mathematically equivalent to the Fourier transform of the impulse response shown in Figure 5d (see Izumo et al., 2016 for another example exploiting this linear property of the system). The EQB contribution to the total sea level on the WCI increases at low frequency, becoming larger than EQD at periods longer than ~280 days (Figure 9). This increase is likely due to the delayed signals passing through the interior of the BoB as RWs radiated from the eastern boundary of the BoB that are increasingly in phase with the faster-traveling signals through the BoB coastal waveguide, which are generated by persistent equatorial wind forcing at longer periods. The EQD contribution, on the other hand, is the largest in the 30–100-day (intraseasonal) band (Figure 9), due to the aforementioned intrinsic timescale of the eastern boundary reflection and the subsequent RW propagation to Sri Lankan coast. EQD decreases as the period becomes longer than the basin adjustment scale, because the east-west gradient of sea level is progressively balanced with the wind stress perturbation at this scale. As a result, the contribution of RWs progressively diminishes, leading to a reduction in the overall magnitude of EQD at the seasonal and interannual timescales.

5. Summary and Discussion

5.1. Summary

In the present work, we investigated the drivers of the baroclinic sea level intraseasonal variability along the WCI. This variability, being related to the thermocline and oxycline depths, has important implications on the coastal ecosystem and fisheries. We focus on baroclinic variability rather than the barotropic response to the MJO discussed by Rohith et al. (2019), as the barotropic mode does not influence the thermocline depth, and has only a minimal effect on near-surface currents.

More specifically, we first investigated whether the "direct connection" (EQD) between the equatorial waveguide and the WCI near Sri Lanka, proposed by Suresh et al. (2013) and Dhage and Strub (2016), exists. We also investigated if the "forcing hotspot" near Sri Lanka, highlighted at seasonal and interannual timescales by Suresh et al. (2016, 2018), does operate effectively at the intraseasonal timescale, as suggested by Amol et al. (2012) and Dhage and Strub (2016).

We first setup idealized experiments using the LCS model as in Suresh et al. (2016) and McCreary et al. (1996), and show that the EQD connection can, at least in principle, exist due to interaction of both forced and reflected equatorial RWs with the coast of Sri Lanka. We further show that the EQD contribution to the WCI sea level weakens if the Sri Lankan landmass is removed. We then setup LCS model with realistic coastline and observed forcing. The 1st EOF of NIO intraseasonal sea level variations simulated by our model is strikingly similar to that of the observations (EOF1 pattern correlation of 0.91 and PC1 correlation of 0.88). By leveraging the linearity of the LCS model, we conducted sensitivity experiments, by imposing Newtonian dampers and special boundary conditions applied in various regions, to break down the NIO sea level into specific processes: EQD, EQB, ST (forcing near southern tip of India and Sri Lanka), BB (Bay of Bengal forcing), and AS (local Arabian Sea forcing).

The largest contributor to the WCI intraseasonal sea level is EQD (regression coefficient of ∼0.4), followed by the EQB (∼0.3), ST (∼0.25), AS (∼0.1) and the BB (∼−0.05) processes. The EQD signal is mainly associated with the interaction of first baroclinic mode, 1–3 meridional modes equatorial RWs with Sri Lanka. We then show that this EQD pathway does not operate effectively at the longer (seasonal and interannual) timescales. At seasonal scale, this is probably partly due to the weaker equatorial zonal wind variations than at the intraseasonal timescale. But most importantly, the diminishing of EQD effect at longer timescales is related to a resonant mechanism that is most efficient at intraseasonal timescales. The travel time of the first baroclinic, first meridional mode equatorial RW between the eastern boundary at Sumatra and the coast of Sri Lanka (around 80°E) is indeed ∼30 days, which is roughly the time it takes for the intraseasonal wind forcing associated with the MJO and monsoon active and break phases to reverse within the equatorial band. The reflected RW is thus reinforced by the RW directly forced by the winds around 80°E, at intraseasonal timescale, but not at the longer timescales (e.g., Han, 2005; Sengupta et al., 2007), resulting in a stronger EQD mechanism at the intraseasonal timescale.

5.2. Discussion

This study builds upon the methodology and findings of Suresh et al. (2013), and consistently reproduces their results regarding the relative contributions of various processes to the WCI sea level ISV. However, it goes a step further by introducing a novel approach to decompose the equatorial signals into EQB (through BoB) and EQD (through direct equatorial and coastal waveguide connection near Sri Lanka) components. This novel approach enabled us to investigate the hypothesis proposed by Suresh et al. (2013) regarding the existence of the EQD connection at the intraseasonal timescale. Dhage and Strub (2016) inferred from observations that this direct connection plays an important role in the WCI sea level ISV. Our results not only validate their hypothesis but also provide a quantitative assessment of its contribution, with regression coefficient of ∼0.4 and ∼0.3 for EQD and EQB, respectively, when regressed against the total intraseasonal sea level.

The second original finding of this study highlights that the EQD is much weaker, but non-negligible, at longer timescales (regression coefficients of 0.1 and 0.2 at the seasonal and interannual timescales, respectively). Consequently, the "leaky waveguide" concept (Shankar et al., 2002; Shetye, 1998) remains valid for the seasonal and interannual timescales. It is only at the intraseasonal timescale the direct connection between the equatorial variability and the WCI becomes apparent. This connection arises because both the wind forcing and the equatorial eastern boundary reflection involve equatorial Rossby meridional modes 1–3 that have significant amplitudes at the latitude of the Sri Lankan coastal waveguide. The third original finding of our study is to

validate the previous hypotheses by Amol et al. (2012) and Dhage and Strub (2016), which proposed that the WCI intraseasonal sea level is influenced by wind variations in the vicinity of Sri Lanka (regression coefficient to the total sea level is ~0.25), as the case for the seasonal (Suresh et al., 2016) and interannual (Suresh et al., 2018) timescale.

The analyses in this paper focuses on the dominant mode of NIO sea level ISV, associated with the MJO during winter and active and break monsoon phases in summer, as previously described by Vialard et al. (2009) and Suresh et al. (2013). However, this large-scale mode is not the sole contributor to the sea level ISV in the NIO, particularly on the WCI. To determine the contributions of each process to the total sea level ISV, we regressed full time series of each process to that of total intraseasonal sea level on the WCI (as opposed to those associated with Figure 7). The individual process contributions using this approach reveals that EQD (0.32 regression coefficient) and ST (0.32) are the major contributors, followed by EQB (0.2), AS (0.17), and BB (0.003). These results provide further confirmation of the strong and consistent EQD connection at the intraseasonal timescale.

Given the significant role of eastern boundary reflection on the EQD process, we examined the impact of its orientation by performing additional LCS model experiments similar to ICTL (see Section 2), but with a lateral boundary that was meridionally oriented at the average location of the equatorial eastern boundary. These experiments revealed that the orientation of eastern boundary had minimal or nearly negligible effect on the EQD process on WCI sea level (results similar to Figure 5d).

Our findings regarding the active EQD connection at the intraseasonal timescale were obtained using a relatively simple, linear ocean model. The EQD and all other processes discussed here should also be present in more sophisticated ocean general circulation models that incorporate non-linear effects, mixed layer dynamics, and thermodynamical processes. However, achieving a clean decomposition of processes with an ocean general circulation model, which is inherently fully non-linear, would probably pose substantial challenges. Nevertheless, we believe that our results can reasonably be trusted based on the similar inferences using observations by, for example, Amol et al. (2012) and Dhage and Strub (2016), as well as the remarkable agreement between the modeled and the observed basin-scale intraseasonal sea level variability.

Data Availability Statement

The authors confirm that the observational data sets used in this study are openly available and their download links are provided in the text. All data sets and software are cited in the paper and listed in the Reference section. LCS model simulations are available from the published papers http://dx.doi.org/10.1002/2016GL069976 and https://doi.org/10.1029/2018GL080972. IDL programming library is available at https://forge.ipsl.jussieu.fr/saxo/download/idldoc_html_output/.

Acknowledgments
IS thanks Director, CSIR-NIO and Vice Chancellor, DUK. IS acknowledges the financial support received from ESSO-INCOIS/MoES (HOOFS) and CSIR, New Delhi. IS also thanks Parvathi Vallivattathillam and Sadhvi Kwatra for their help with figures and useful discussions. JV, ML, and TI are funded by Institut de Recherche pour le Développement (IRD) and they acknowledge the funding support from the CNES (Centre National d'Etudes Spatiales) AltiKa project. They also acknowledge IRD for supporting regular visits to CSIR-NIO. JV thanks CSIR-NIO for his "Adjunct Scientist" position during 2016–2019. This is NIO contribution 7200.

References

Amol, P., Shankar, D., Aparna, S. G., Shenoi, S. S. C., Fernando, V., Shetye, S. R., et al. (2012). Observational evidence from direct current measurements for propagation of remotely forced waves on the shelf off the west coast of India. *Journal of Geophysical Research*, *117*(C5), C05017. https://doi.org/10.1029/2011JC007606

Chelton, D. B., DeSzoeke, R. A., Schlax, M. G., El Naggar, K., & Siwertz, N. (1998). Geographical variability of the first baroclinic Rossby radius of deformation. *Journal of Physical Oceanography*, *28*(3), 433–460. https://doi.org/10.1175/1520-0485(1998)028<0433:gvotfb>2.0.co;2

Chen, G., Wang, D., & Hou, Y. (2012). The features and interannual variability mechanism of mesoscale eddies in the Bay of Bengal. *Continental Shelf Research*, *47*, 178–185. https://doi.org/10.1016/j.csr.2012.07.011

Cui, W., Yang, J., & Ma, Y. (2016). A statistical analysis of mesoscale eddies in the Bay of Bengal from 22–year altimetry data. *Acta Oceanologica Sinica*, *35*(11), 16–27. https://doi.org/10.1007/s13131-016-0945-3

Currie, J. C., Lengaigne, M., Vialard, J., Kaplan, D. M., Aumont, O., Naqvi, S. W. A., & Maury, O. (2013). Indian Ocean dipole and El Niño/southern oscillation impacts on regional chlorophyll anomalies in the Indian Ocean. *Biogeosciences*, *10*, 6677–6698. https://doi.org/10.5194/bg-10-6677-2013

Dhage, L., & Strub, P. T. (2016). Intra-seasonal sea level variability along the west coast of India. *Journal of Geophysical Research: Oceans*, *121*(11), 8172–8188. https://doi.org/10.1002/2016JC011904

Gopalakrishna, V. V., Rao, R. R., Nisha, K., Girishkumar, M. S., Pankajakshan, T., Ravichandran, M., et al. (2008). Observed anomalous upwelling in the Lakshadweep Sea during the summer monsoon season of 2005. *Journal of Geophysical Research*, *113*(C05001), 1–12. https://doi.org/10.1029/2007JC004240

Goswami, B. N. (2005). South Asian monsoon. In W. K. M. Lau, & D. E. Waliser (Eds.), *Intraseasonal variability in the atmosphere-ocean climate system* (pp. 19–55). Springer. https://doi.org/10.1007/b138817

Han, W. (2005). Origins and dynamics of the 90-day and 30–60-day variations in the equatorial Indian Ocean. *Journal of Physical Oceanography*, *35*(5), 708–728. https://doi.org/10.1175/JPO2725.1

Han, W., McCreary, J. P., Masumoto, Y., Vialard, J., & Duncan, B. (2011). Basin resonances in the equatorial Indian Ocean. *Journal of Physical Oceanography*, *41*(6), 1252–1270. https://doi.org/10.1175/2011JPO4591.1

Izumo, T., & Colin, M. (2022). Improving and harmonizing El Niño recharge indices. *Geophysical Research Letters*, *49*(23), e2022GL101003. https://doi.org/10.1029/2022gl101003

Izumo, T., Vialard, J., Dayan, H., Lengaigne, M., & Suresh, I. (2016). A simple estimation of equatorial Pacific response from windstress to untangle Indian Ocean Dipole and Basin influences on El Niño. *Climate Dynamics*, *46*(7–8), 2247–2268. https://doi.org/10.1007/s00382-015-2700-4

Le Blanc, J. L., & Boulanger, J. P. (2001). Propagation and reflection of long equatorial waves in the Indian Ocean from TOPEX/POSEIDON data during the 1993-1998 period. *Climate Dynamics*, *17*(7), 547–557. https://doi.org/10.1007/s003820000128

Masumoto, Y., Hase, H., Kuroda, Y., Matsuura, H., & Takeuchi, K. (2005). Intraseasonal variability in the upper layer currents observed in the eastern equatorial Indian Ocean. *Geophysical Research Letters*, *32*(2), L02607. https://doi.org/10.1029/2004GL021896

Mccreary, J. P., Han, W., Shankar, D., & Shetye, S. R. (1996). Dynamics of the East India coastal current. 2. Numerical solutions. *Journal of Geophysical Research*, *101*(c6), 13993–14010. https://doi.org/10.1029/96JC00560

McCreary, J. P., Kundu, P. K., & Molinari, R. (1993). A numerical investigation of dynamics, thermodynamics and mixed-layer processes in the Indian Ocean. *Progress in Oceanography*, *31*(3), 181–244. https://doi.org/10.1016/0079-6611(93)90002-U

Murtugudde, R., McCreary, J. P., & Busalacchi, A. J. (2000). Oceanic processes associated with anomalous events in the Indian Ocean with relevance to 1997–1998. *Journal of Geophysical Research*, *105*(C2), 3295–3306. https://doi.org/10.1029/1999JC900294

Nagura, M., & McPhaden, M. J. (2012). The dynamics of wind-driven intraseasonal variability in the equatorial Indian Ocean. *Journal of Geophysical Research*, *117*(C2), C02001. https://doi.org/10.1029/2011JC007405

Naqvi, S. W. A., Naik, H., Jayakumar, D. A., Pratihary, A. K., Narvenkar, G., Kurian, S., et al. (2009). Seasonal anoxia over the western Indian continental shelf. In J. D. Wiggert, R. R. Hood, S. W. A. Naqvi, K. H. Brink, & S. L. Smith (Eds.), *Indian ocean: Biogeochemical processes and ecological variability*. American Geophysical Union. https://doi.org/10.1029/2008GM000745

Naqvi, S. W. A., Naik, H., Jayakumar, D. A., Shailaja, M. S., & Narvekar, P. V. (2006). Seasonal oxygen deficiency over the western continental shelf of India. In *Past and present water column anoxia* (pp. 195–224). Springer Netherlands.

Parvathi, V., Suresh, I., Lengaigne, M., Ethe, C., Vialard, J., Levy, M., et al. (2017). Positive Indian Ocean Dipole events prevent anoxia along the west coast of India. *Biogeosciences*, *14*(6), 1541–1559. https://doi.org/10.5194/bg-14-1541-2017

Prakash, S., Prakash, P., & Ravichandran, M. (2013). Can oxycline depth be estimated using sea level anomaly (SLA) in the northern Indian Ocean? *Remote Sensing Letters*, *4*(11), 1097–1106. https://doi.org/10.1080/2150704X.2013.842284

Praveen Kumar, B., Vialard, J., Lengaigne, M., Murty, V. S. N., McPhaden, M. J., Cronin, M., et al. (2013). TropFlux wind stresses over the tropical oceans: Evaluation and comparison with other products [Dataset]. Climate Dynamics, *40*(7–8), 2049–2071. https://doi.org/10.1007/s00382-012-1455-4

Rohith, B., Paul, A., Durand, F., Testut, L., Prerna, S., Afroosa, M., et al. (2019). Basin-wide sea level coherency in the tropical Indian Ocean driven by Madden–Julian Oscillation. *Nature Communications*, *10*(1), 1257. https://doi.org/10.1038/s41467-019-09243-5

Saji, N. H., Goswami, B. N., Vinayachandran, P. N., & Yamagata, T. (1999). A dipole mode in the tropical Indian Ocean. *Nature*, *401*(6751), 360–363. https://doi.org/10.1038/43854

Schott, F. A., & McCreary, J. P. (2001). The monsoon circulation of the Indian Ocean. *Progress in Oceanography*, *51*, 1–123. https://doi.org/10.1016/s0079-6611(01)00083-0

Sengupta, D., Senan, R., Goswami, B. N., & Vialard, J. (2007). Intraseasonal variability of equatorial Indian Ocean zonal currents. *Journal of Climate*, *20*(13), 3036–3055. https://doi.org/10.1175/JCLI4166.1

Shankar, D., McCreary, J. P., Han, W., & Shetye, S. R. (1996). Dynamics of the East India coastal current: 1. Analytic solutions forced by interior Ekman pumping and local alongshore winds. *Journal of Geophysical Research*, *101*(C6), 13975–13991. https://doi.org/10.1029/96JC00559

Shankar, D., & Shetye, S. R. (1997). On the dynamics of the Lakshadweep high and low in the southeastern Arabian Sea. *Journal of Geophysical Research*, *102*(C6), 12551–12562. https://doi.org/10.1029/97JC00465

Shankar, D., Vinayachandran, P. N., & Unnikrishnan, A. S. (2002). The monsoon currents in the north Indian Ocean. *Progress in Oceanography*, *52*(1), 63–120. https://doi.org/10.1016/S00796611(02)00024-1

Shetye, S. R. (1998). West India coastal current and Lakshadweep high/low. *Sadhana*, *23*(5–6), 637–651. https://doi.org/10.1007/bf02744586

Suresh, I., Vialard, J., Izumo, T., Lengaigne, M., Han, W., McCreary, J., & Muraleedharan, P. M. (2016). Dominant role of winds near Sri Lanka in driving seasonal sea level variations along the west coast of India. *Geophysical Research Letters*, *43*(13), 7028–7035. https://doi.org/10.1002/2016GL069976

Suresh, I., Vialard, J., Lengaigne, M., Han, W., McCreary, J., Durand, F., & Muraleedharan, P. M. (2013). Origins of wind-driven intraseasonal sea level variations in the North Indian Ocean coastal waveguide. *Geophysical Research Letters*, *40*(21), 5740–5744. https://doi.org/10.1002/2013GL058312

Suresh, I., Vialard, J., Lengaigne, M., Izumo, T., Parvathi, V., & Muraleedharan, P. M. (2018). Sea level interannual variability along the west coast of India. *Geophysical Research Letters*, *45*(22), 12440–12448. https://doi.org/10.1029/2018GL080972

Vialard, J., Shenoi, S. S. C., McCreary, J. P., Shankar, D., Durand, F., Fernando, V., & Shetye, S. R. (2009). Intraseasonal response of the northern Indian Ocean coastal waveguide to the Madden-Julian oscillation. *Geophysical Research Letters*, *36*(14), L14606. https://doi.org/10.1029/2009GL038450

Webber, B. G., Matthews, A. J., Heywood, K. J., & Stevens, D. P. (2012). Ocean Rossby waves as a triggering mechanism for primary Madden–Julian events. *Quarterly Journal of the Royal Meteorological Society*, *138*(663), 514–527. https://doi.org/10.1002/qj.936

Webster, P. J., Moore, A. M., Loschnigg, J. P., & Leben, R. R. (1999). Coupled oceanic atmospheric dynamics in the Indian Ocean during 1997–98. *Nature*, *401*(6751), 356–360. https://doi.org/10.1038/43848

Yu, W., Xiang, B., Liu, L., & Liu, N. (2005). Understanding the origins of interannual thermocline variations in the tropical Indian Ocean. *Geophysical Research Letters*, *32*(24), 24706. https://doi.org/10.1029/2005GL024327

Zhang, C. (2005). Madden-Julian oscillation. *Reviews of Geophysics*, *43*, RG2003. https://doi.org/10.1029/2004RG000158

References From the Supporting Information

Locarnini, R. A., Mishonov, A. V., Antonov, J. I., Boyer, T. P., Garcia, H. E., Baranova, O. K., et al. (2010). World Ocean Atlas 2009, volume 1: Temperature [Dataset]. In S. Levitus (Ed.), *NOAA Atlas NESDIS* (Vol. 68, p. 184). U.S. Government Printing Office. Retrieved from https://www.ncei.noaa.gov/sites/default/files/2020-04/woa09_vol1_text.pdf

Smith, W. H. F., & Sandwell, D. T. (1997). Global sea floor topography from satellite altimetry and ship depth soundings [Dataset]. Science, *277*, 1956–1962. https://doi.org/10.1126/science.277.5334.1956